SCIENTIFIC REPORTS

OPEN

SUBJECT AREAS:
ELECTRONIC PROPERTIES AND DEVICES
ELECTRONIC PROPERTIES AND MATERIALS

Received
27 January 2014

Accepted
11 March 2014

Published
10 April 2014

Correspondence and requests for materials should be addressed to S.C.R. (Raysc@unisa.ac.za) or W.F.P. (wfpong@mail.tku.edu.tw)

The Effect of Thermal Reduction on the Photoluminescence and Electronic Structures of Graphene Oxides

C.-H. Chuang[1], Y.-F. Wang[1], Y.-C. Shao[1], Y.-C. Yeh[2], D.-Y. Wang[2], C.-W. Chen[2], J. W. Chiou[3], Sekhar C. Ray[4], W. F. Pong[1], L. Zhang[5], J. F. Zhu[5] & J. H. Guo[6]

[1]Department of Physics, Tamkang University, Tamsui 251, Taiwan, [2]Department of Material Science and Engineering, National Taiwan University, Taipei 106, Taiwan, [3]Department of Applied Physics, National University of Kaohsiung, Kaohsiung 811, Taiwan, [4]Department of Physics, College of Science, Engineering and Technology, University of South Africa, Private Bag X6, Florida, 1710, Science Campus, Christiaan de Wet and Pioneer Avenue, Florida Park, Johannesburg, South Africa, [5]National Synchrotron Radiation Laboratory, University of Science and Technology of China, Hefei230029, China, [6]Advanced Light Source, Lawrence Berkeley National Laboratory, Berkeley, California 94720, USA.

Electronic structures of graphene oxide (GO) and hydro-thermally reduced graphene oxides (rGOs) processed at low temperatures (120–180°C) were studied using X-ray absorption near-edge structure (XANES), X-ray emission spectroscopy (XES) and resonant inelastic X-ray scattering (RIXS). C *K*-edge XANES spectra of rGOs reveal that thermal reduction restores C = C sp^2 bonds and removes some of the oxygen and hydroxyl groups of GO, which initiates the evolution of carbonaceous species. The combination of C *K*-edge XANES and K_α XES spectra shows that the overlapping π and π* orbitals in rGOs and GO are similar to that of highly ordered pyrolytic graphite (HOPG), which has no band-gap. C K_α RIXS spectra provide evidence that thermal reduction changes the density of states (DOSs) that is generated in the π-region and/or in the gap between the π and π* levels of the GO and rGOs. Two-dimensional C K_α RIXS mapping of the heavy reduction of rGOs further confirms that the residual oxygen and/or oxygen-containing functional groups modify the π and σ features, which are dispersed by the photon excitation energy. The dispersion behavior near the *K* point is approximately linear and differs from the parabolic-like dispersion observed in HOPG.

After the discovery of graphene[1–3], significant effort has been applied to graphene oxide (GO), because GO is an important intermediate in the preparation of graphene, which has a wide range of applications[4]. GO can be visualized as sheets of graphene that are decorated with oxygen and/or oxygen-containing functional groups on both the basal planes and edges. The presence of oxygen makes GO amenable to chemical functionalization without significant disruption of the sp^2 network of the graphene hexagonal lattice. Thermally reduced graphene oxide (rGO) is the most attractive method for the conversion of GO to graphene, because it is simple, reliable, high yield and low cost[5–12]. Carrying out the reduction process at a relatively high annealing temperature (≥200°C) reportedly restores rGO from GO[7,9,10]. However, this high-temperature process is unlikely to be compatible with the fabrication techniques used for most electronics, hence thermal reduction at a lower temperature (120–180°C) has been proposed. Although not effective in entirely reducing the residual oxygen and/or oxygen-containing functional groups in GO, low-temperature de-oxygenating processes are very useful for patterning the reduced graphene on glass or plastic substrates for electronic applications, as well as for synthesizing a wide range of functional hybrids that can be used in polymer composites, biosensors, energy storage and conversion technologies[13].

An earlier study reported the presence of various amounts of residual oxygen and/or oxygen-containing functional groups in rGO, the electrical conductivity of which reaches several orders of magnitude lower than that of mechanically exfoliated graphene[14]. Both rGO and GO have been shown theoretically to possess a band-gap that can be tuned over a large range of energies, suggesting that the functionalization of graphene by oxidation can alter its electronic properties[15,16]. Optical investigations have also found that GO exhibits a band-gap that can be tuned by varying the degree of oxidation or reduction and that reduction changes the intensity of various photoluminescence (PL) features[9,17]. Additionally, it has been suggested that rGO exhibits a mixture of sp^2 and sp^3 bonds that depends on the degree of reduction[18]; furthermore, the electrical transport behavior changes from

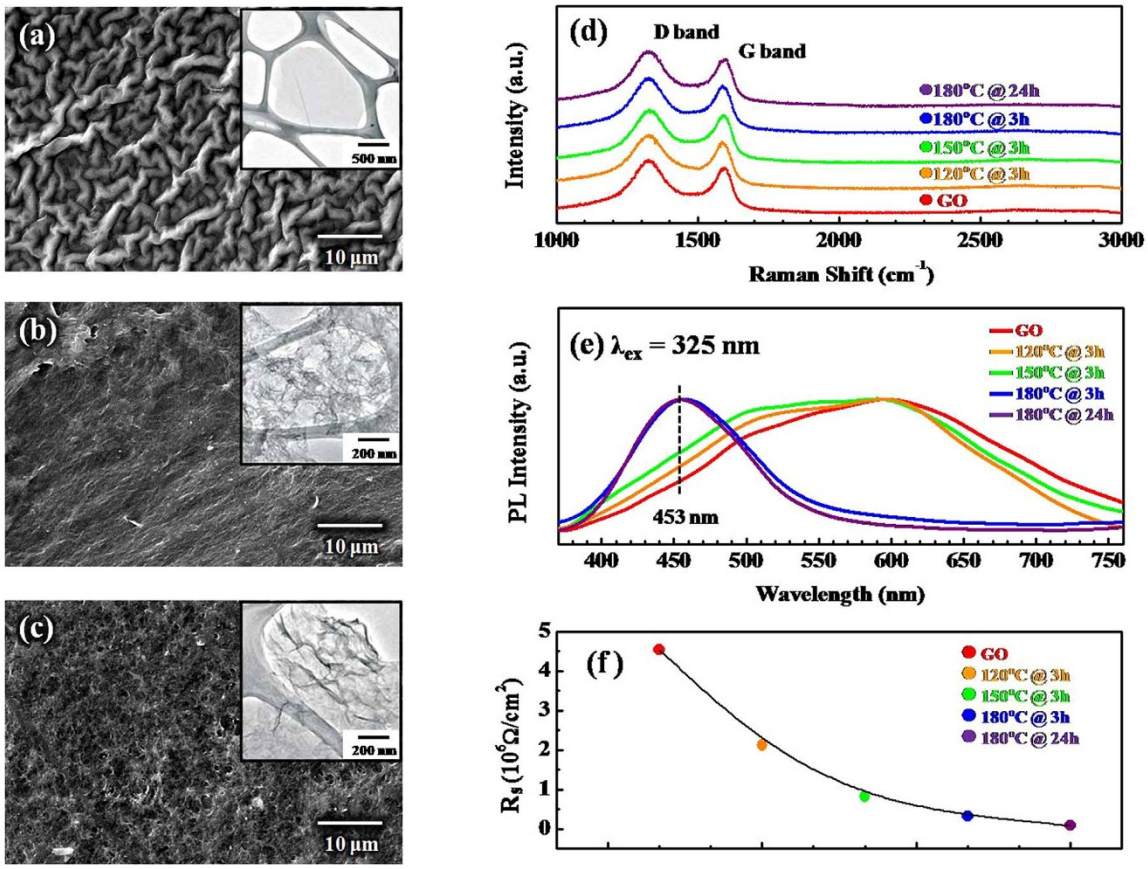

Figure 1 | SEM images of (a) the as-synthesized GO, (b) the rGO formed at 150°C@3 hr, and (c) the rGO formed at 180°C@24 hr. The insets show the respective TEM images. (d) The Raman spectra were obtained at an excitation wavelength of 633 nm. (e) The normalized photoluminescence spectra of the GO and rGOs reduced at different temperatures for different periods, and (f) the sheet resistances of the GO and rGOs reduced at different temperatures for different periods.

insulator-hopping-like to semimetal-band-like as the number of localized π states increases[19]. Reduced graphene oxide exhibits the restoration of the C = C sp^2 bond, as in the graphene hexagonal lattice, as a result of the removal of oxygen and/or oxygen-containing functional groups, thereby forming carbonaceous (CO_2 and/or CO) species[9,10]; as a result, hole defects are etched within the graphene basal plane. To date, little is known about the persistence of the residual oxygen and/or oxygen-containing functional groups. Several questions, such as how generated defects modify the electronic structures or band dispersions close to the Fermi level (E_f) or Dirac (***K***) point, as well as how these defects are related to the PL and electronic transport properties of rGO, remain to be answered[20].

This study investigates how various stages of low-temperature (120–180°C) reduction influence the electronic and bonding states in rGOs and GO, and how changes in these stages are closely correlated with the PL and electrical properties of these materials. C and O *K*-edge X-ray absorption near-edge structure (XANES), X-ray emission spectroscopy (XES) and resonant inelastic X-ray scattering (RIXS) spectroscopy were utilized extensively to elucidate various reduction processes. Changes in the PL and electrical sheet resistivity (R_s) of rGOs and GO with various degrees of reduction are examined herein. Our results reveal the low-temperature evolution of the bonding states, the electronic structures and band dispersions near E_f or the ***K*** point, and the PL and R_s of the rGOs and GO.

Results and Discussion

Figures 1(a)–(c) and their insets present scanning electron microscopy (SEM) and transmission electron microscopy (TEM) images of the as-synthesized GO and rGOs formed at 150°C@3 h and 180°C@24 h, respectively. The surface morphology of GO is noodle-like, while that of the rGOs is wrinkle-like. Raman spectroscopy, a well-known non-destructive method for determining the quality of graphene, yields two features, namely, the G-band and the D-band. However, the two main Raman features in the spectra of the GO and rGOs in Figure 1(d), which was recorded following various reduction processes, are as follows: the G-band at approximately 1587 cm^{-1} is attributed to the E_{2g} phonon of sp^2 states, and the D-band at approximately 1327 cm^{-1} is attributed to the A_{1g} symmetry and indicates disorder in the graphene lattice that is caused by the defects in the form of vacancies and grain boundaries[21–23].

The ratio (I_D/I_G) of the intensity of the D-band to that of the G-band of the GO (which reveals the sp^2/sp^3 ratio) does not differ significantly from that of the rGOs. The near equality of these I_D/I_G ratios may be related to the structural distortion/defects, surface rippling and wrinkle-structures that are seen in the SEM images in Figures 1(a)–(c); these features are formed in the graphene lattice by the restoration of C sp^2 bonds and by de-oxidation upon hydrothermal treatment, such that the intensity ratio of (I_D/I_G) is intact[24] and insensitive to thermal reduction. Mattevi *et al.*[9] also observed no significant variation of the I_D/I_G ratio of annealed rGOs with annealing temperatures up to 1000°C, even though different oxygen-containing functional groups were removed from the GO.

In contrast to the Raman spectra results, the evolution of the PL spectra of these samples shows a significant change following the conversion of GO to rGOs with various hydrothermal reductions, as shown in Figure 1(e). The PL spectra of GO and the weakly reduced rGOs (120°C@3 h and 150°C@3 h) show asymmetric broad lineshapes, ranging from 400 to 800 nm. In contrast, the strongly

reduced rGOs (180°C@3 h and 180°C@24 h) predominantly exhibit one main feature that is centered at approximately 453 nm. The result is consistent with the mechanism proposed by Chien *et al.*[23], which was developed to explain the evolution of PL spectra from the original yellow-red color in the as-synthesized GO solution to blue in the rGO solution, following the application of the photothermal reduction technique. The original GO consists of a significant number of disorder-induced defect states within the $\pi-\pi^*$ gap and exhibits a predominant broad PL spectrum centered at longer wavelengths. After deoxygenation, the number of disorder-induced states within the $\pi-\pi^*$ gap decreases, and an increased number of small sp^2 clusters in the rGO result in blue luminescence. This transition occurs because the hydrothermal method is a relatively strong reduction process compared to the photothermal reduction method. Thus, no gradual transition from GO to rGO is observed in the hydrothermal reduction process, as compared to those observed in the milder photothermal reduction precess[23].

Notably, the X-ray excited optical photoluminescence (XEOL) that was observed in earlier studies by the authors also demonstrated that the PL behavior was closely related to the number of sp^2 clusters and the density of states (DOSs) within the π and π* gap in N-doped graphene nanoflakes (GNFs:N)[25]. Figure 1(f) plots R_s following various reduction steps. Clearly, R_s decreases gradually from its maximum value of approximately $4.5 \times 10^6\ \Omega/cm^2$ (GO) to its minimum value of approximately $1 \times 10^5\ \Omega/cm^2$ (for the most heavily reduced rGO 180°C@24 h). The decrease of the R_s of GO/rGOs with increasing thermal reduction temperature and duration supports the fact that the process of reduction is carried out by the removal of oxygen and/or oxygen-containing functional groups and is based on the restoration of the C = C sp^2 bonds in the graphene hexagonal lattice, as mentioned above, which also improves the electrical conductivity of the rGOs.

Although the most heavily reduced rGO (180°C@24 h) has a relatively high value of R_s, the low-temperature reduction processes that are applied herein cannot remove all residual oxygen and/or oxygen-containing functional groups, so sp^3 bonds and defects still form in the graphene basal plane[9,10]. These sp^3 bonds and defects can disrupt the transport of charge carriers through graphene sp^2 networks and/or discontinuities between the sp^2 domains, reducing electron mobility and the electrical conductivity of rGOs. Accordingly, electron transport in rGOs may occur by hopping rather than near ballistic transport, as in the case of mechanically exfoliated graphene[26,27]. This phenomenon further explains why the electrical conductivity of GO/rGOs is several orders of magnitude lower than that of mechanically exfoliated graphene[14].

Figure 2 displays the normalized C *K*-edge XANES spectra of the rGOs, GO and the reference HOPG. The C *K*-edge XANES spectra in the figures have been divided by the incident intensity I_0 and then normalized to have the same area in the energy range from 296–298 eV, following the application of the standard procedure for background subtraction. The features $\mathbf{C_1}$ and $\mathbf{C_5}$ at approximately 285.5 and 292 eV in the C *K*-edge XANES spectra of HOPG are attributed to the C $1s \rightarrow \pi^*$ and $1s \rightarrow \sigma^*$ transitions, respectively. The π*-feature ($\mathbf{C_1}$) is typical of the out-of plane C = C or graphitic sp^2 bond, while the in-plane σ*-feature ($\mathbf{C_5}$) is typical of the C-C bond[25,28]. In contrast, a similar line-shape and position of the HOPG can be seen relative to those of the σ*-feature ($\mathbf{C_5}$) in the GO and rGOs, whereas the π*-feature ($\mathbf{C_1}$) is shifted 0.4 eV below and 0.1 eV above the GO and rGOs, respectively, relative to that of HOPG, as indicated by the dashed line in Figure 2. The lower energy of the π*-feature ($\mathbf{C_1}$) in the GO spectrum relative to that of the rGOs can be attributed either to the high degree of structural rearrangement of the aromatic ring that is decorated with the oxygen-containing functional groups[14] or to the effect of edge/defect states[29].

Additionally, both the rGOs and GO have σ*-features ($\mathbf{C_5}$) that are of almost equal intensity, while the intensity of the π*-feature

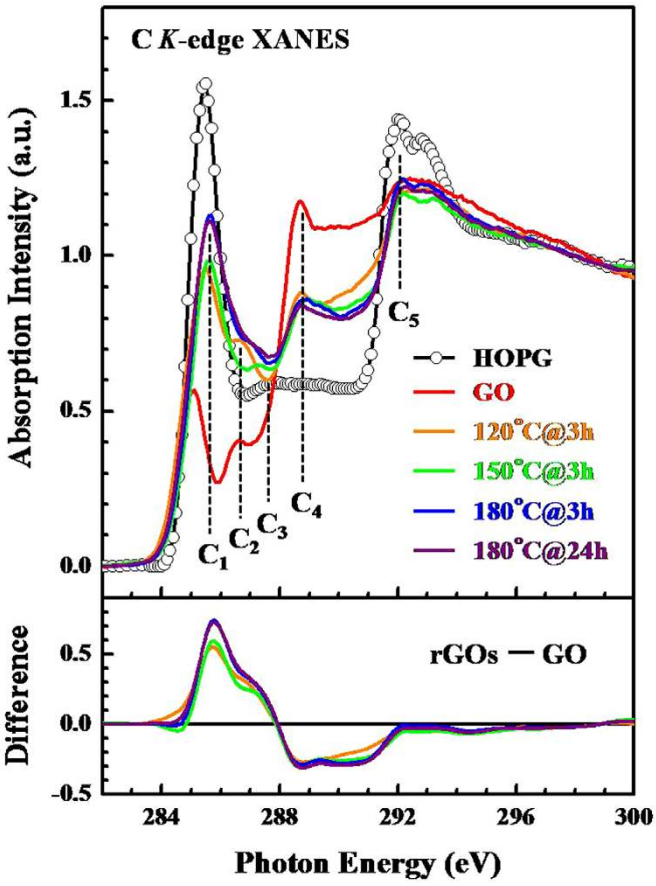

Figure 2 | XANES spectra of the GO and rGOs at the C *K*-edge. The bottom panels show the difference between the rGOs and GO.

($\mathbf{C_1}$) of the rGOs not only is significantly greater than that of GO but also gradually increases with the thermal temperature and duration, indicating an increase in the restoration of C = C or sp^2-bonding with the degree of reduction steps. The $\mathbf{C_2}$–$\mathbf{C_4}$ wide-features in the range from 286–289 eV are also observed between the π* and σ* features, as shown in Figure 2. Although the assignment of these features to specific states has been controversial[30], they are typically attributed to carbon that is bound to oxygen and hydrogen, and specifically to π*(C-OH) at approximately 286.6 eV, to π*(C-O-C) at approximately 287.9 eV and to π*(C = O) in the -COOH bond at approximately 288.7 eV[25,29,31]. The intensities of the $\mathbf{C_2}$–$\mathbf{C_4}$ features of the rGOs differ significantly from those of GO, and the intensities of the $\mathbf{C_2}$ and $\mathbf{C_3}$ (feature $\mathbf{C_4}$) features of the rGOs are significantly greater (less) than those of GO.

The lower panel presents the difference spectra of the rGOs and GO, indicating that the conversion of GO to rGOs increases the number of π*(C-OH) ($\mathbf{C_2}$) and π*(C-O-C) ($\mathbf{C_3}$) bonds but reduces the number of the formation of π*(C = O) ($\mathbf{C_4}$) bonds in -COOH. More careful examination of the C *K*-edge XANES spectra of the rGOs demonstrates that despite the variation in the degree of reduction of rGOs (ranging from weak for 120°C@3 h and 150°C@3 h to heavy reduction for 180°C@3 h and 180°C@24 h) with varying temperature and duration, the C = C or sp^2-bonds are restored and the number of π*(C-OH) bonds increases slightly with the number of reduction steps. In contrast, the features of π*(C-O-C) and the π*(C = O) bond in -COOH remain almost unchanged with the further reduction of the rGOs. These results suggest that C = C sp^2- and π*(C-OH) bonds depend more strongly on the reduction temperature and duration than the π*(C-O-C) and π*(C = O) bonds in -COOH. At low temperatures (120-180°C), the reduction process does not always lead to the complete desorption of oxygen and/or

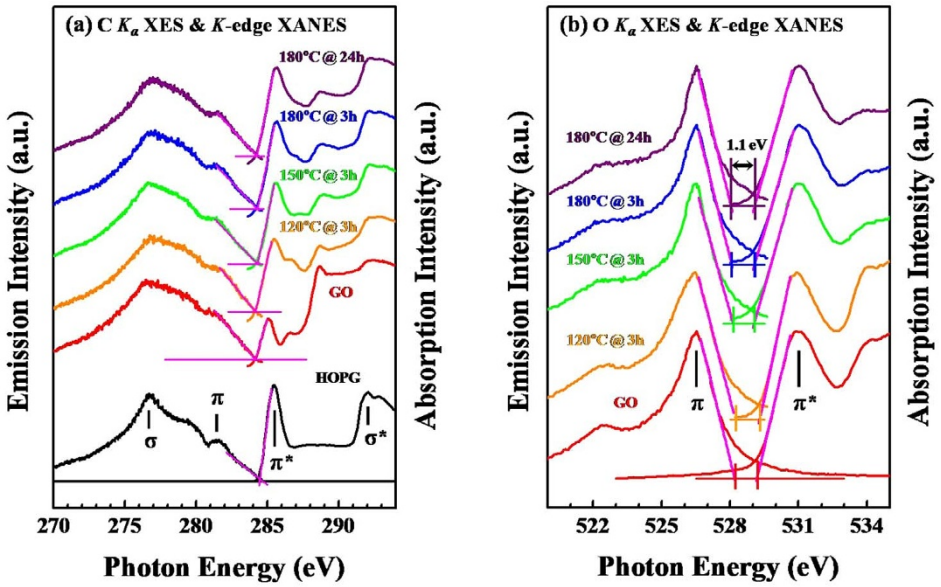

Figure 3 | (a) The normalized C *K*-edge XANES and K_α XES spectra of the GO, rGOs and HOPG. (b) The normalized O *K*-edge XANES and K_α XES spectra of the GO and rGOs.

oxygen-containing functional groups in thermal annealing. This observation has been presented in previous studies of the thermal reduction of GO by similar means; these studies also revealed the removal of oxygen and hydroxyl groups with the evolution of carbonaceous species[9,10].

Figures 3(a) and 3(b) present the C and O *K*-edge XANES and K_α XES spectra of rGOs, GO and reference HOPG, respectively. The π and σ bands in the C (O) *K*-edge XES spectra are observed at 278–284 eV (526–528 eV) and 270–278 eV (522–526 eV)[25,31–33], respectively, as shown in Figure 3(a) [Fig. 3(b)], with an incident photon energy of 310 eV (560 V). The general line-shapes in the C (O) K_α XES spectra in Figure 3(a) [Fig. 3(b)] are similar for the rGOs and GO. All spectra exhibit a broad feature, which is associated with the σ state and centered at approximately 276.7 eV (522.5 eV), as well as a high-energy shoulder, which is associated with the π state and centered close to 281.5 eV (526.5 eV). Both leading edges of the C *K*-edge XANES and the corresponding K_α XES spectra were extrapolated to the baseline to determine the conduction-band-minimum (E_{CBM}) and valence-band-maximum (E_{VBM})[25,31,34], respectively, as well as the energy of the band-gap.

The two extrapolated lines in the C *K*-edge XANES and K_α XES spectra in Figure 3(a) intersect each other, which is similar to that of metallic HOPG, indicating that rGOs and GO have no band-gap with a lower density of state crossing the Fermi level throughout. However, in contrast, as presented in Figure 3(b), the energy separation between the O π* and the π state of the rGOs and GO, derived from the leading edges of the O *K*-edge XANES and K_α XES spectra, is approximately 1.1 eV. Pristine graphene has a zero band-gap, as does a semimetal, meaning that the highest occupied (E_{VBM}) and lowest unoccupied (E_{CBM}) states coincide at the ***K*** point, which was at approximately 284.7 eV in the C *K*-edge XANES and K_α XES spectra of the graphene[33]. The dispersions of the two corresponding energy bands of graphene are essentially linear close to the ***K*** point[35,36], unlike those of conventional semiconductors, which are parabolic dispersions near E_{VBM} and the E_{CBM}.

Combining the results in Figures 3(a) and 3(b) suggests that C atoms, rather than O atoms, contribute most to the local DOSs of the C 2*p*-derived states close to the E_{CBM} and E_{VBM} of rGOs and GO, and specifically to the π* and π orbitals close to the ***K*** point. The C *K*-edge XANES and K_α XES spectra reveal no band-gap in the rGOs and GO, similar to metallic HOPG, regardless of the fact that the R_s values of rGOs and GO are higher, on the order of 10^5–10^6 Ω/cm^2, as shown in Figure 1(f), suggesting that the R_s values of rGOs and GO are significantly affected by residual oxygen and/or the fraction of oxygen-containing functional groups through the disruption of the C = C network. According to the C *K*-edge XANES in Figure 2, the GO clearly has a smaller (larger) fraction of C = C sp^2-bonds (associated with the oxygen-containing functional group, C = O bonds in COOH-bond that terminates the edge and/or basal plane of graphene) than reduced the rGOs, as addressed above, and hence has a higher R_s value. Introducing O atoms can disrupt the C = C π network, causing a weak perturbation of the linear π orbitals close to the ***K*** point, which reduces the connectivity of the C π electron network in the graphene plane. Nevertheless, based on the C *K*-edge XANES and K_α XES spectra, the perturbation that is caused by oxygen or oxygen-containing functional groups apparently does not generate the band-gap near the ***K*** point in the rGOs or GO. In contrast, previous studies have reported that GO contains sp^3 carbon atoms that are saturated with oxygen, forming local carbon-oxygen bonds, which open a small band-gap[37–39].

As stated above, various thermal reductions significantly change PL behaviors during the conversion of GO to rGOs, as presented in Figure 1(e). The significant effect of reduction on PL emission is associated with induced changes in the electronic structures and local DOSs within the π and π* gap, indicating that the O atoms play an important role in changing the PL features, similar to the N atoms in GNFs:N[25]. The variation of the PL emission of rGOs and GO can result in the incorporation of oxygen into C sites, forming carbon-oxygen bonds and oxygen-containing functional groups in the graphene lattice, where these sites may act as energy traps. Because the bonding of many O atoms and oxygen-containing functional groups to graphene in GO and the weak reduction of rGOs lead to the transfer of resonance energy from the O to the C sp^2 clusters in the graphene lattice, the radiative recombination rate is increased, yielding broad emission features in the PL spectra in Figure 1(e). As the temperature and duration of thermal reduction are increased, oxygen-containing functional groups are gradually removed, reducing the transfer of resonance energy from the O sites to the sp^2 clusters in the graphene lattice. Consequently, the rate of radiative recombination is reduced, narrowing the PL emission and the main feature at approximately 453 nm, which presents with a weak shoulder at 510 nm.

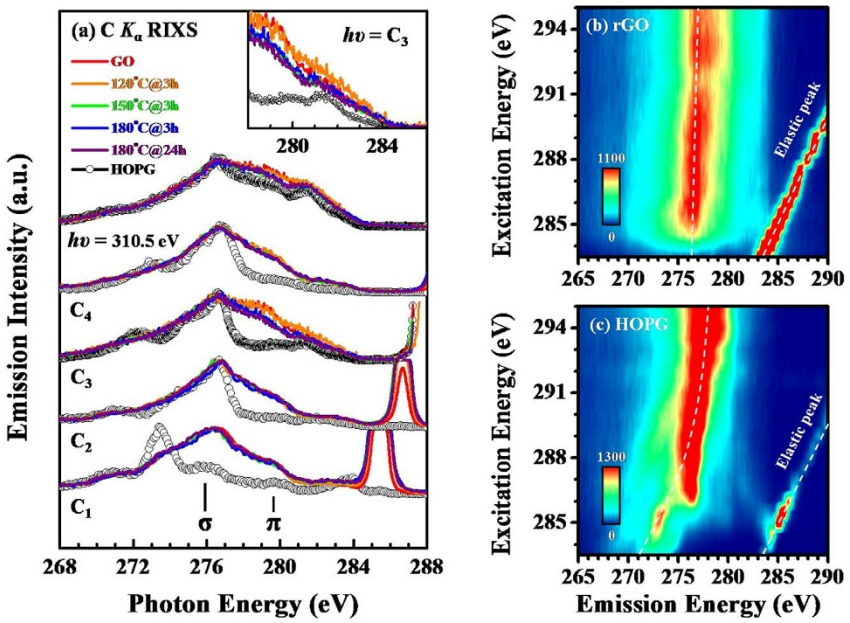

Figure 4 | (a) The normalized C K_α RIXS spectra of the GO, rGOs and HOPG obtained by excitation at photon energies of 285.5 eV (**C$_1$**), 286.6 eV (**C$_2$**), 287.9 eV (**C$_3$**), 288.7 eV (**C$_4$**) and 310.5 eV. Notably, the resonance features in the lower right-hand corner are the elastic peaks. (b) 2d-RIXS mapping of rGO (180°C@24 h) and (c) HOPG as functions of both the excitation and emission energies.

The above arguments are principally based on a study of the enhancement of the broad luminescence emission from 400 to 800 nm in the PL spectra, which is caused by the CO-related electronic states in the oxygen plasma-treated mechanically exfoliated graphene[40]. However, the C *K*-edge XANES spectra show that the low-temperature (120–180°C) reduction process by which the rGOs are formed does not always remove all of the oxygen and oxygen-containing functional groups from the GO but that the process can increase the number of π*(C-OH) and π*(C-O-C) bonds upon the rearrangement of oxygen and oxygen-containing functional groups with carbon; this consequence may also play a role in enhancing the transfer of resonance energy from O sites to the sp^2 clusters in the graphene lattice, which results in broad PL emission. Alternatively, the change in the PL features from the GO to the weakly reduced rGOs to the heavily reduced rGOs, as presented in Figure 1(e), can be caused by the optical transitions that involve a significant number of oxygen-induced localized states in the band tail of the π-π* gap, thereby confirming the reduction of oxygen-containing functional groups in the rGOs that have undergone various degrees of reduction, according to the C K_α RIXS spectra. This observation further demonstrates the decrease in the number of local DOSs from GO through the weakly reduced rGOs to the heavily reduced rGOs. Specifically, the valence DOSs of the rGOs in the π region and/or in the gap between π and π* are lower than that of GO.

Figure 4(a) displays the C K_α RIXS spectra of the GO, rGOs and HOPG, obtained by excitation at the photon energies of **C$_1$**–**C$_4$** in Figure 2, which correspond specifically to the excitations of C = C (285.5 eV), C-OH (286.6 eV), C-O-C (287.9 eV) and C = O, respectively, in the -COOH (288.7 eV) bonds. For comparison, the C K_α XES spectra of the GO, rGOs and HOPG collected with an incident photon energy ($h\nu$) of 310.5 eV are also presented for the incoherent fraction as a sum over the valence band contribution. All of the emission spectra in Figure 4(a) were acquired within the same period and were normalized to unity for the maximum inelastic emission peak in each spectrum. According to RIXS theory, total energy and momentum must be conserved in resonant inelastic scattering during absorption-emission processes. The $h\nu$-dependent emission features obtained from HOPG result from a transition at a well-orientated crystal momentum[41,42].

These dispersive features between the σ and π orbitals and their lineshapes generally vary distinctly from each other. In principle, the π emission is caused by transitions from p_z states that are oriented perpendicular to the graphene plane. Emission from the σ bands is significantly more isotropic, because these bands are derived in part from the p_x and p_y states that reside parallel to the surface. Apparently, the C K_α XES spectra of the rGOs, GO and HOPG that were obtained at an excitation energy of $h\nu$ = 310.5 eV exhibit similar line-shapes, whereas the π-feature of the C K_α RIXS spectra of the rGOs/GO change with incident photon energies from **C$_1$** to **C$_4$**, as presented in Figure 4(a), in a very different way from those of HOPG, because the excitation energies at the different absorption edges of carbons that are bonded to oxygen and/or oxygen-containing functional groups generate more resonant π-features in the rGOs/GO than in HOPG. The regions of the π states and/or the π-π* gap provide direct evidence that the emission spectral intensities of rGOs/GO are larger than that of HOPG for all of the considered excitation energies, **C$_1$**–**C$_4$**, revealing that the incorporation of oxygen and/or oxygen-containing functional groups into the graphene lattice increases the number of oxygen and/or oxygen-containing functional group-induced states above that in HOPG; the DOSs in the π-region and/or in the gap between π and π* are increased, as well.

Importantly, the spectra in Figure 4(a) further show that the spectral intensities of GO and the weakly reduced rGOs (120°C@3 h and 150°C@3 h) exceed those of the heavily reduced of rGOs (180°C@3 h and 180°C@24 h) for excitation energies $h\nu$ of 287.9 eV (**C$_3$**), 288.7 eV(**C$_4$**) and 310.5 eV.

The upper inset in Figure 4(a) magnifies the feature in the π region and was obtained at an excitation energy of 287.9 eV, clearly verifying that upon thermalization, the de-oxidation of GO reduces the proportion of induced states that are formed by the oxygen and/or oxygen-containing functional groups. In particular, the valence DOSs in the π region and/or in the gap between π and π* significantly decreases from GO through the weakly reduced rGOs to the heavily reduced rGOs. Based on excitation at the absorption edges (C_1 - C_4), the RIXS spectra reflect the coherent scattering of the carbon site and its corresponding oxygen functional groups, showing the similar band structure profiles of each, although at the *off*-absorption position ($h\nu$ = 287.9 eV); furthermore, the up-increase in the π region is

understood based on the reduction of the coherent contribution with the enhancement of the oxygen-induced interference.

With respect to the pristine graphene network, the rest of the oxygen bonds in the rGOs act as perturbing or interacting sites, significantly enhancing photon-electron scattering. This result consistently elucidates the variation of the PL behaviors shown in Figure 1(e) and the number of oxygen- and/or oxygen-containing group-induced localized states within the π-π* gap, which is likely the higher electron-hole recombination rate for PL phenomena. Notably, at an excitation energy of $h\nu$ = 285.5 eV ($\mathbf{C_1}$) or 286.6 eV ($\mathbf{C_2}$), as shown in Figure 4(a), the line-shapes and intensities of the π-state do not differ significantly between the GO/weakly reduced rGOs and the heavily reduced rGOs, although the excitation energy at the absorption edges [energies $\mathbf{C_1}$ and $\mathbf{C_2}$ in Fig. 2(a)] of C = C and the oxygen-containing functional group C-OH vary significantly, possibly because the emission feature occurs at an energy close to that of the prominent elastic peaks, entangling the induced states[33]. Therefore, the intensity of the feature associated with the oxygen- and/or oxygen-containing group-induced DOSs in the C K_α RIXS spectra of GO do not differ significantly from those of the rGOs that have undergone various thermal reduction processes.

Figures 4(b) and 4(c) plot the two-dimensional (2d) C K_α RIXS maps as functions of both emission and excitation energies for the most heavily reduced rGO (180°C@24 h) and HOPG, respectively. The color profile reveals the dispersive π and σ bands in terms of emission intensity and with excited series from 284 to 295 eV. The features in the lower right-hand corner of the figure are known to be due to the elastic peaks. The 2d-RIXS spectra in Figure 4(b) clearly reveal that the band dispersion of the π and σ features is essentially linear near the ***K*** point based on the use of a selective excitation energy with the wave vectors in rGO (180°C@24 h); these spectra also differ from the parabolic-like dispersion at values greater than excitations of 285 eV in HOPG [Fig. 4(c)]. This result indicates a difference between the band dispersions of the π and σ orbitals of rGO and those of HOPG, which is likely due to the presence of either a single or a few layers of graphene sheets and the oxygen-mediated influence in the rGO (180°C@24 h). It is shown above that the C *K*-edge XANES and K_α XES spectra of GO and rGO overlap, indicating metallic behavior, similar to HOPG. This may be due to the formation of a graphene domain or clusters in some area within the GO and rGO matrix that consequently exhibits metallic behavior. Again, the O *K*-edge XANES and K_α XES spectra do not overlap and show only a small energy separation. This observation could be due to the formation of C = O and/or C-OH bonds and is responsible for the photoluminescence behavior. Importantly, the 2d-RIXS of rGO (180°C@24 h) further demonstrates that although oxygen and/or oxygen-containing functional groups are incorporated into the graphene lattice, thereby disrupting the C = C π network and causing a weak perturbation, the linear-like band dispersion of π and σ near the ***K*** point remains like that of graphene, suggesting that the electronic properties in rGOs can be tailored through functionalization by reducing the oxygen from GO.

In summary, the various PL emission and electrical transport phenomena observed in GO and rGOs are closely related to the electronic structures and bonding states of these materials, which are determined by the incorporation of oxygen and/or oxygen-containing functional groups into the graphene lattice. Various reduction processes remove some oxygen-containing functional groups in the graphene lattice, significantly reducing or eliminating the intensity of the PL features and also decreasing the number of valence DOSs in the π region and/or in the gap between π and π* from the GO or the weakly reduced rGOs to the heavily reduced rGOs obtained from the XANES/XES results. Further C K_α 2d-RIXS mapping of the rGO confirms that the residual oxygen and/or oxygen-containing functional groups modify the π and σ features, in a manner that varies from that of HOPG. This study finds that the characteristics of PL emission and the electrical properties of GO/rGOs can be tailored through functionalization by the reduction of oxygen, rendering GO/rGOs attractive for use in novel optoelectronic devices.

Methods

Preparation of GO and rGOs. GO was synthesized by the oxidation of graphite using a modification of Hummers' method[4]. Using de-ionized water, purified GO was diluted to the concentration required for further use. Twenty milliliters of GO-solution with a concentration of 1 mg/ml were transferred to a Teflon-lined autoclave. The pH of the solution was adjusted to 6.5 by the addition of 0.01 M sulfuric acid. Hydrothermal treatments were conducted at various annealing temperatures (120–180°C) and durations (3–24 hrs). The rGOs obtained, with the functional group of GO deactivated[43], are denoted as 120°C@3 h, 150°C@3 h, 180°C@3 h and 180°C@24 h. The chemically modified rGOs were washed using de-ionized water for purification. To fabricate the samples for lateral analysis, all purified rGOs were deposited on Si substrates by drop casting at 100°C.

Characterizations. XANES, XES and RIXS measurements were performed at undulator beamlines 7.0.1 and 8.0.1 at the Advanced Light Source (ALS), Lawrence Berkeley National Laboratory. The C and O *K*-edge XANES spectra of the rGOs and GO were recorded in the total electron yield mode at room temperature. The energy resolution of the absorption spectra was set to 0.1 eV. The energy resolution of the XES and RIXS spectra was set to approximately 0.35 eV. The absorption and emission spectra were calibrated using highly ordered pyrolytic graphite (HOPG).

1. Geim, A. K. Graphene: Status and Prospects. *Science* **324**, 1530–1534 (2009).
2. Novoselov, K. S. *et al.* Two-dimensional gas of massless dirac fermions in graphene, *Nature* **438**, 197–200 (2005).
3. Geim, A. K. & Novoselov, K. S. The rise of graphene, *Nature Materials* **6**, 183–191 (2007).
4. Hummers Jr, W. S. & Offeman, R. E. Preparation of graphitic oxide, *J. Am. Chem. Soc.* **80**, 1339–1339 (1958).
5. Feng, H., Cheng, R., Zhao, X., Duan, X. & Li, J. A low-temperature method to produce highly reduced graphene oxide. *Nature Commun.* **4**, 1539–1545 (2013).
6. Stankovich, S. *et al.* Synthesis of graphene-based nanosheets via chemical reduction of exfoliated graphite oxide. *Carbon* **45**, 1558–1565 (2007).
7. Eda, G., Fanchini, G. & Chhowalla, M. Large-area ultrathin films of reduced graphene oxide as a transparent and flexible electronic material. *Nature Nanotechnol.* **3**, 270–274 (2008).
8. Yang, D. *et al.* Chemical analysis of graphene oxide films after heat and chemical treatments by X-ray photoelectron and Micro-Raman spectroscopy. *Carbon* **47**, 145–152 (2009).
9. Mattevi, C. *et al.* Evolution of Electrical, chemical and structural properties transparent and conducting chemically derived graphene thin films. *Adv. Func. Mater.* **19**, 2577–2583 (2009).
10. Bagri, A. *et al.* Structural evolution during the reduction of chemically derived graphene oxide, *Nature Chem.* **2**, 581–587 (2010).
11. Lee, V. *et al.* Large-area chemically modified graphene films: Electrophoretic deposition and characterization by soft x-ray absorption spectroscopy. *Chem. Mater.* **21**, 3905–3916 (2009).
12. Shin, H. J. *et al.* Efficient reduction of graphite oxide by sodium borohydrilde and Its effect on electrical conductance. *Adv. Func. Mater.* **19**, 1987–1992 (2009).
13. Sharma, S. *et al.* Rapid microwave synthesis of CO tolerant reduced graphene oxide -supported platinum electrocatalysts for oxidation of methanol. *J. Phys. Chem. C* **114**, 19459–19466 (2010).
14. Jung, I., Dikin, D. A., Piner, R. D. & Ruoff, R. S. Tunable eectrical conductivity of individual graphene oxide sheets reduced at "Low" temperatures. *Nano Letters* **8**, 4283–4287 (2008).
15. Yan, J.-A., Xian, L. & Chou, M. Y. Structural and electronic properties of oxidized graphene. *Phys. Rev. Lett.* **103**, No. 086802,1–4 (2009).
16. Yan, J.-A. & Chou, M. Y. Oxidation functional groups on graphene: Structural and electronic properties. *Phys. Rev. B* **82**, No. 125403, 1–10 (2010).
17. Eda, G. *et al.* Blue photoluminescence from chemically derived graphene Oxide. *Adv. Mater.* **22**, 505–509 (2010).
18. Luo, Z., Vora, P. M., Mele, E. J., Johnson, A. T. C. & Kikkawa, J. M. Photoluminescence and band gap modulation in graphene oxide. *Appl. Phys. Lett.* **94**, 111909,1–3 (2009).
19. Eda, G., Mattevi, C., Yamaguchi, H., Kim, H. & Chhowalla, M. Insulator to semimetal transition in graphene oxide. *J. Phys. Chem. C* **113**, 15768–15771 (2009).
20. Acik, M. *et al.* The role of intercalated water in multilayered graphene oxide. *ACS Nano* **4**, 5861–5868 (2010).
21. Ferrari, A. C. & Robertson, J. Interpretation of raman spectra of disordered and amorphous carbon. *Phys. Rev. B* **61**, 14095–14107 (2000).
22. Ferrari, A. C. *et al.* Raman spectrum of graphene and graphene layers. *Phys. Rev. Lett.* **97**, 187401,1–4 (2006).
23. Chien, C. T. *et al.* Tunable photoluminescence from Graphene Oxide. *Angew. Chem. Int. Ed.* **51**, 6662–6666 (2012).

24. Zhang, L. *et al.* Electronic structure study of ordering and interfacial interaction in graphene/Cu composites. *Carbon* **50**, 5316–5322 (2012).
25. Chiou, J. W. *et al.* Nitrogen functionalized graphene nanoflakes (GNFs:N): Tunable photoluminescence and electronic Structures. *J. Phys. Chem. C* **116**, 16251–16258 (2012).
26. Neto, A. H. C., Guinea, F., Peres, N. M. R., Novoselov, K. S. & Geim, A. K. The electronic properties of graphene. *Rev. Mod. Phys.* **81**, 109–162 (2009).
27. Du, X., Skachko, I., Barker, A. & Andrei, E. Y. Approaching ballistic transport in suspended graphene. *Nature Nanotech.* **3**, 491–495 (2008).
28. Pao, C. W. *et al.* Change of structural behaviors of organo-silane exposed graphene nanoflakes. *J. Phys. Chem. C* **114**, 8161–8166 (2010).
29. Zhou, J. G. *et al.* Nano-scale chemical imaging of a single sheet of reduced graphene oxide. *J. Mater. Chem.* **21**, 14622–14630 (2011).
30. Hua, W., Gao, B., Li, S., Ågren, H. & Luo, Y. X-ray absorption spectra of graphene from first-principles simulations. *Phys. Rev. B* **82**, 155433–155439 (2010).
31. Chang, C.-K. *et al.* Band gap engineering of chemical vapor deposited graphene by *in Situ* BN Doping. *ACS Nano* **7**, 1333–1341 (2013).
32. Rajasekaran, S., Kaya, S., Anniyev, T., Ogasawara, H. & Nilsson, A. Probing substrate effects in the carbon-projected band structure of graphene on Pt(111) through resonant inelastic x-ray scattering. *Phys. Rev. B* **85**, 045419,1–5 (2012).
33. Zhang, L. *et al.* Electronic band structure of graphene from resonant soft x-ray spectroscopy: The role of core-hole effects. *Phys. Rev. B* **86**, 245430,1–5 (2012).
34. Ray. *et al.* Graphene Supported Graphone/Graphane Bilayer Nanostructure Material for Spintronics. *Sci. Rep.* **4**, 3862:1–7 (2014).
35. Wallace, P. R. The band theory of graphite. *Phys. Rev.* **71**, 622–634 (1947).
36. Slonczewski, J. C. & Weiss, P. R. Band structure of graphite. *Phys. Rev.* **109**, 272–279 (1958).
37. Elias, D. C. *et al.* Control of graphene's properties by reversible hydrogenation: evidence for graphane. *Science* **323**, 610–613 (2009).
38. Park, S. & Ruoff, R. S. Chemical methods for the production of graphenes. *Nat. Nanotechnol.* **4**, 217–224 (2009).
39. Balog, R. *et al.* Bandgap opening in graphene induced by patterned hydrogen adsorption. *Nat. Mater.* **9**, 315–319 (2010).
40. Gokus, T. *et al.* Making graphene luminescent by oxygen plasma treatment. *ACS Nano* **3**, 3963–3968 (2009).
41. Skytt, P. *et al.* Angle-resolved soft-x-ray fluorescence and absorption study of graphite. *Phys. Rev. B* **50**, 10457–10461 (1994).
42. Carlisle, J. A. *et al.* Probing the graphite band structure with resonant soft-x-ray fluorescence. *Phys. Rev. Lett.* **74**, 1234–1237 (1995).
43. Zhou, Y., Bao, Q., Tang, L. A. L., Zhong, Y. & Loh, K. P. Hydrothermal dehydration for the "Green" reduction of exfoliated graphene oxide to graphene and demonstration of tunable optical limiting properties. *Chem. Mater.* **21**, 2950–2956 (2009).

Acknowledgments

The authors C.-H.C. and W.F.P. acknowledge the National Science Council of Taiwan for financial support under Contract No. NSC NSC99-2119-M032-004-MY3 and NSC 102-2112-M-032-001. The author S.C.R. acknowledges the National Research Foundation, South Africa, for financial support. The author J.-F. Zhu receives support from the National Basic Research Program of China (2010CB923302, 2013CB834605), the Natural Science Foundation of China (Grant No. 21173200), and the Specialized Research Fund for the Doctoral Program of Higher Education (SRFDP) of the Ministry of Education (Grant No. 20113402110029). The Advanced Light Source is supported by the Director, Office of Science, Office of Basic Energy Sciences, of the U.S. Department of Energy under Contract No. DE-AC02-05CH11231.

Author contributions

C.-H.C., S.C.R. and W.F.P. designed the experiments with an initial discussion with C.-W.C. The GO and rGOs were synthesized by Y.-C.Y., D.-Y.W. and C.-W.C. All measurements were performed by C.-H.C., Y.-F.W., Y.-C.S., L.Z. and J.W.C. The data were analyzed and the manuscript was prepared by C.-H.C., S.C.R. and W.F.P. The manuscript was modified by J.F.Z., J.H.G. All authors discussed the results and contributed to the finalization of the manuscript.

Additional information

Competing financial interests: The authors declare no competing financial interests.

How to cite this article: Chuang, C.-H. *et al.* The Effect of Thermal Reduction on the Photoluminescence and Electronic Structures of Graphene Oxides. *Sci. Rep.* **4**, 4525; DOI:10.1038/srep04525 (2014).